narra j

Original Article

Design of lipid nanoparticle (LNP) containing genetic material CRISPR/Cas9 for familial hypercholesterolemia

I GNJA. Prasetia[1,2], Neng F. Kurniati[3], Catur Riani[1] and Diky Mudhakir[1*]

[1]Department of Pharmaceutics, School of Pharmacy, Institut Teknologi Bandung (ITB), Bandung, Indonesia; [2]Pharmacist Profession Study Program, Faculty of Math and Natural Sciences, Universitas Udayana, Bali, Indonesia; [3]Department of Pharmacology-Clinical Pharmacy, School of Pharmacy, Institut Teknologi Bandung (ITB), Bandung, Indonesia

*Corresponding author: mudhakir@itb.ac.id

Abstract

Familial hypercholesterolemia is a genetic disorder caused by mutations in the low-density lipoprotein receptor gene (*LDLR*) and the current treatment still focuses on symptom management. The aim of this study was to develop a lipid nanoparticle (LNP)-based delivery system for the CRISPR/Cas9 component in correcting *LDLR* gene mutations. LNPs were prepared using an ultrasonic-solvent emulsification technique by varying the surfactant: oil ratio (SOR), homogenization speed and time, and sonication time. Next, the LNP surface was modified by adding DSPE-PEG_{2000}-NH_2 and polyethyleneimine. The next stage is to design the single guide RNA (sgRNA) and Donor DNA wildtype (Donor DNA wt). This genetic material was complexed with LNP and then transfected into Hepa1-6 *LDLR* mt cells, an in vitro representation of cells suffering from familial hypercholesterolemia. This optimization process produced LNPs with a particle size of 118.6±0.8 nm and a polydispersity index of 0.34±0.03. The LNP surface modification resulted in a zeta potential of +7.5 mV. A transmission electron microscope (TEM) analysis showed spherical morphology with size distribution following a regular pattern. LNP cell viability tests showed good biocompatibility at concentrations <15 mM with a half-maximal inhibitory concentration (IC_{50}) value of 27.7 mM. The dominant cellular uptake mechanism of LNP was through the clathrin-mediated endocytosis (CME) pathway. The Hepa1-6 *LDLR* mt cell model was successfully produced with the transfecting agent Lipofectamine 3000 by homology-directed repair (HDR) mechanism. The LNP-genetic material complex with a ratio of sgRNA:Cas9:Donor DNA wt (1:1:0.04) showed an increase in *LDLR* gene expression of 3.3±0.2 times and *LDLR* protein levels reached 12.95±0.25 ng/mL on day 4 after transfection. The results of this study indicate that the developed LNP-based delivery system has the potential for gene therapy applications in familial hypercholesterolemia.

Keywords: Familial hypercholesterolemia, gene therapy, CRISPR/Cas9, LDLR protein, lipid nanoparticle

https://narraj.org/

Introduction

Familial hypercholesterolemia is a genetic disorder characterized by low-density lipoprotein receptor gene (*LDLR*) mutations, affecting mainly hepatocyte cells. This genetic disorder can result in impaired cholesterol metabolism and increase the risk of premature cardiovascular disease [1,2]. Although there have been advances in lipid-lowering therapies, current treatments of familial hypercholesterolemia focus more on managing symptoms rather than addressing the

Received: February 4, 2025 - Accepted: April 10, 2025 - Published online: April 15, 2025

underlying genetic cause [1-5]. The emergence of CRISPR/Cas9 gene editing technology has opened new possibilities for developing targeted genetic therapies for familial hypercholesterolemia [6-10]. However, successfully delivering CRISPR/Cas9 components to hepatocyte cells remains a critical challenge, necessitating the development of efficient and safe delivery systems. One aspect considered is the particle size, where the success of drug delivery systems targeting liver cells is ≤150 nm [11-14].

Lipid nanoparticles (LNP) have emerged as promising carriers for the delivery of genetic material, offering advantages such as biodegradability, biocompatibility, and the ability to protect nucleic acids from degradation [15,16]. Designing LNP-based delivery systems requires careful optimization of various parameters, including particle size, surface charge, and lipid composition, to achieve efficient cellular uptake and therapeutic effectiveness. Recent advances in LNP formulation techniques have demonstrated their potential to deliver CRISPR/Cas9 components. However, the development of optimized systems for specific genetic disorders such as familial hypercholesterolemia remains an active area of research [16-18].

Successful implementation of CRISPR/Cas9-based gene therapy for familial hypercholesterolemia depends on several critical factors, such as the design of effective single guide RNA (sgRNA) and Donor DNA sequences, development of appropriate carriers, and demonstration of efficient gene editing in target cells [8,13,14,19]. Optimization of these components requires a systematic approach to understanding their individual and combined effects on therapeutic outcomes. Previous studies have shown that the efficiency of CRISPR/Cas9-mediated gene editing can significantly influence the delivery system's characteristics and the genetic component's precise design [18,20].

The aim of this study was to optimize LNP formulation parameters for effective CRISPR/Cas9 delivery to enhance gene-editing efficiency for *LDLR* correction in familial hypercholesterolemia model cells. Understanding these factors is crucial for developing effective therapeutic strategies for familial hypercholesterolemia and other genetic disorders requiring hepatic gene editing. In the present study, a comprehensive approach was employed to develop an LNP-based delivery system containing CRISPR/Cas9, designed to enhance the stability of genetic material and maintain its gene-editing capability, particularly for mutated *LDLR* genes. The optimization strategy included refining the surfactant-to-oil ratio (SOR), adjusting mixing conditions, and modifying the LNP surface by incorporating DSPE-PEG2000-NH_2 and polyethyleneimine (PEI) [16,21,22]. This combination improved cellular uptake while protecting the encapsulated genetic material. In addition, establishing an effective in vitro model system is essential for evaluating the potential of the LNP-based delivery system. Therefore, hepatocyte cells were used as an in vitro test model, including Hepa1-6 wild-type (Hepa1-6 wt) cells and Hepa1-6 *LDLR* mutation (Hepa1-6 *LDLR* mt) cells. These Hepa1-6 *LDLR* mt cells harbour *LDLR* gene mutations that mimic familial hypercholesterolemia-affected cells' characteristics and provide a valuable platform for assessing the efficacy of the LNP-CRISPR/Cas9 system [23-26]. This in vitro model enabled a systematic evaluation of gene-editing efficiency, cellular uptake mechanisms, and the restoration of *LDLR* gene function through various molecular and cellular analyses. The findings from this study may provide valuable insights into the design of more effective delivery systems for CRISPR/Cas9-based therapeutics and contribute to the advancement of genetic treatments for hereditary disorders.

Methods

Study design and setting

An experimental study was conducted to optimize and characterize LNP formulations for efficient CRISPR/Cas9 delivery, focusing on physicochemical properties, including morphology, particle size, and zeta potential. An in vitro study was conducted to evaluate the gene-editing potential of the LNP-CRISPR/Cas9-Donor DNA wt system (LNP complex) in Hepa1-6 *LDLR* mt cells, assessing *LDLR* gene expression via qRT-PCR and *LDLR* protein levels using ELISA.

The study commenced with LNP production using an ultrasonic-solvent emulsification technique, optimizing parameters such as the surfactant-to-oil ratio (SOR), homogenization speed and duration, and sonication time. LNPs were then characterized for their physicochemical

properties, including morphology, particle size, polydispersity index, zeta potential, and optical properties using TEM. Functional group characterization was performed via Fourier transform infrared (FTIR) spectroscopy. Additionally, entrapment efficiency, LNP viability, and cellular uptake assays were conducted using Hepa1-6 wt cells as the hepatocyte cells model. Furthermore, sgRNA and Donor DNA wildtype (Donor DNA wt) were designed as key components of the CRISPR/Cas9 system, playing a crucial role in the gene-editing process.

The produced LNPs were complexed with genetic material to form LNP-CRISPR/Cas9-Donor DNA wt (LNP complex). Then, the value of the N/P ratio is calculated by calculating the positive charge of cationic lipids (N) and the negative charge of nucleic acids (P). This value is related to the LNP transfection efficiency. LNP complex was then transfected to Hepa1-6 *LDLR* mt cells. These mutant cells were generated by inducing mutations in Hepa1-6 wt cells, specifically targeting exon 4 of the *LDLR* gene on chromosome 9 (GeneID: 16835), using the transfection agent Lipofectamine 3000. Hepa1-6 *LDLR* mt cells serve as a model for familial hypercholesterolemia, exhibiting key characteristics of decline in *LDLR* gene expression and reduced LDLR protein levels compared to normal Hepa1-6 wt cells. By delivering CRISPR/Cas9 and Donor DNA wt via LNPs into Hepa1-6 *LDLR* mt cells, the gene-editing process was expected to correct the mutation, leading to the formation of revertant cells in which *LDLR* gene expression and LDLR protein levels return to normal.

Design of the sgRNA and Donor DNA wt as components of genetic material

In this study, sgRNA and protospacer adjacent motif (PAM) were used in the sequence GGGGCTGCTAACGCCTTTGG(AGG), as previously tested [23]. Cas9 protein (Cat. #0000127048, Sigma Aldrich, St. Louis, MO, USA) was diluted with the provided buffer to a final concentration of 170 ng/µL. The Donor DNA wt was designed using the Invitrogen TrueDesign Genome Editor (https://apps.thermofisher.com/apps/genome-editing-portal/#/select/experiment) to replace damaged DNA sequences in the gene-editing process. The Donor DNA wt was synthesized with homology arm lengths of ~0.1 to 0.5 kb, as longer arms do not increase the efficiency [27-29]. The sequence of the Donor DNA wt used for gene editing in Hepa1-6 *LDLR* mt cells was GAC GGC TCC GAT GAG TGG CCA CAG AAC TGC CAG GGC CGA GAC ACG GCC TCC AAA GGC GTT AGC AGC CCC TGC TCC TCC CTG GAG TTC CAC TGT GGT AGC AGT **GAG** TGT ATC CAT CGC AGC TGG GTC TGT GAC GGC GAG GCA GAC TGC AAG GAC AAG TCA GAT GAG GAG CAC TGC GCG GTG GCC ACC TGC CGA CCT GAT GAA TTC CAG. Both sgRNA and Donor DNA wt were synthesized by Integrated DNA Technologies (IDT, Coralville, IA, USA) at concentrations of 340 ng/µL for sgRNA and 3.4 ng/µL for Donor DNA wt. These components were incubated at room temperature for 30 minutes before use. The efficiency of Donor DNA wt in gene editing through the CRISPR/Cas9 system was assessed using Tracking of Insertion, Deletions, and Recombination (TIDER) (http://shinyapps.datacurators.nl/tider/) [30].

Production of LNP and characterizations

Before the production of LNP, a series of tests were conducted, including optimizing SOR and the time and speed of the Homogenizer Ultra-turrax (IKA, Beijing, China) and Sonicator Probe (Labman, Rajasthan, India). Additional information is available in the underlying data (**Table S1**, **S2**, and **S3**).

The LNP production was carried out via an ultrasonic-solvent emulsification technique, where the water phase (containing PEI and Tween 80 (all from Sigma-Aldrich, St. Louis, Missouri, MO, USA)) and the oil phase (containing squalene, glyceryl trimyristate, DOTAP, and Span 60 (all from Sigma-Aldrich, St. Louis, Missouri, MO, USA)) were stirred using a hot plate stirrer (IKA, Beijing, China) at 50°C and 500 rpm for 20 minutes [18,31]. The two phases were then homogenized at 7200 rpm for 5 minutes. After thorough mixing, particle size reduction was performed by sonication at 60% amplitude for 20 minutes. DSPE-PEG2000-NH2 was added to the LNP formulation, and the mixture was incubated at 4°C for 15 minutes [31,32].

Particle size analysis (PSA) and surface charge measurement

PSA and polydispersity index (PDI) were used to determine the distribution and size of LNPs using Photon Correlation Spectroscopy (PCS) with a Delsa Nano Series instrument (Beckman Coulter, Pasadena, CA, USA). The principle of this instrument is based on measuring the rate of

fluctuations in laser light intensity scattered by particles as they diffuse through a fluid [33]. For zeta potential measurement, the sample was vortexed and diluted fivefold in a 10 mM sodium citrate trihydrate buffer. The solution was then placed into a cuvette and analyzed using a Nano Particle Analyzer, Horiba SZ-100 (Horiba Ltd, Kyoto, Japan).

Characterization of functional groups

Functional groups of the LNP were characterized using a FTIR spectrophotometer IR Prestige-21 (Shimadzu, Tokyo, Japan) and analyzed in the 4,000–1,300 cm^{-1} range. The absorbance values were compared, showing the absorption in the functional group area [34].

Size and morphological analysis

The size and morphology of LNPs were analyzed using a TEM, Hitachi HT7700 (Hitachi, Tokyo, Japan) at 120 kV. Particle diameters were measured using ImageJ software (National Institutes of Health and Laboratory for Optical and Computational Instrumentation, University of Wisconsin, USA) [34].

Entrapment efficiency assay

The entrapment efficiency of CRISPR/Cas9 components was determined using the RiboGreen assay [32]. LNPs complexed with sgRNA were centrifuged (16,000×g for 15 minutes) to separate free sgRNA. The supernatant was analyzed using the Quant-iT RiboGreen RNA Assay Kit (ThermoFisher Scientific, Shanghai, China) according to the manufacturer's protocol. A microplate reader measured fluorescence intensity at excitation/emission wavelengths of 485/528 nm [35]. The entrapment efficiency percentage (%EE) was calculated using the following equation: %EE=((total sgRNA–sgRNA free)/total sgRNA)×100%.

LNP viability assay

Hepa1-6 wt cells were cultured in a 96-well plate with 5×10^3 cells/well. Cells were incubated with DMEM (Gibco, Billings, MT, USA) containing LNP at various concentrations for 24 hours. A 3-(4,5-dimetil-2-tiazolil)-2,5-difeniltetrazolium bromide (MTT) kit (Invitrogen, Carlsbad, CA, USA) was used to determine the cells' viability, and the absorbance was measured at 450 nm [36]. Untreated cells were used as a reference (negative control), and cells with Tween 20 (5%) solution were used as a positive control [37].

Cellular uptake efficiency assay

The cellular uptake mechanism was analyzed qualitatively using confocal laser scanning microscopy (CLSM) Olympus FV1200 (Olympus, Tokyo, Japan). LNP was modified with 1,1′-dioctadecyl-3,3,3′,3′-tetramethylindotricarbocyanine perchlorate (DiD) (Invitrogen, Carlsbad, CA, USA). It was used to observe the effect of adenosine triphosphate (ATP) on the cellular uptake process. DiD has a fluorescence at Ex/Em=644/665 nm. Cells were grown in a confocal dish with a 1×10^5 cells/well density for 24 hours. Next, the cells were transfected with LNP-DiD for 1 hour, and then the cell nuclei were stained using Hoechst 33342 (Invitrogen, Carlsbad, CA, USA) for 15 minutes. The LNP cellular uptake was calculated by incubating cells at 4°C and 37°C, representing ATP-independent (non-endocytosis) and ATP-dependent (endocytosis) processes, respectively [38]. To calculate the cellular uptake, the intensity of DiD fluorescence was measured semi-quantitatively using ImageJ software (National Institutes of Health and Laboratory for Optical and Computational Instrumentation, University of Wisconsin, USA) [39].

Classification of the uptake mechanism

The endocytosis uptake mechanism was assessed using specific endocytosis pathway inhibitors. The inhibitors used were 0.4 M sucrose for clathrin-mediated endocytosis (CME), 5 µg/mL filipin III (Sigma Aldrich, St. Louis, MO, USA) for caveolae-mediated endocytosis (CvME), and 0.1 mM amiloride for the macropinocytosis pathway as recommended [40]. Briefly, Hepa1-6 wt cells were grown with a density of 1×10^5 cells/well and incubated at 37°C for 24 hours. The cells were transfected with each inhibitor for 30 minutes and treated with LNP-DiD for 1 hour. Cells were washed and stained with Hoechst 33342 (Invitrogen, Carlsbad, CA, USA) for 15 minutes. Cellular uptake efficiency was calculated semi-quantitatively by measuring the intensity of DiD

fluorescence using ImageJ software (National Institutes of Health and Laboratory for Optical and Computational Instrumentation, University of Wisconsin, USA) [39].

Production of LNP complex

The genetic materials (sgRNA, Cas9, and Donor DNA wt) were mixed into the LNP and incubated at 4°C for 30 minutes (**Table S4**). The N/P ratio, the ratio between the positive charge of nitrogen (N) from cationic components such as cationic lipids and the negative charge of phosphate groups (P) in genetic material, was then calculated [45]. The purpose of calculating the N/P ratio is to optimize the entrapment efficiency and delivery of genetic material into the cell. LNP complex was stored at 2–8°C before use.

Production of Hepa1-6 *LDLR* mt cell for in vitro model

Hepa1-6 wt cells culture

Hepa1-6 cells were obtained from PAMITRAN-UP (Pusat Akademik, Inovasi, Teknologi, dan Riset Kesehatan, Universitas Padjadjaran, Bandung, Indonesia). Cell cultures were grown in a complete growth medium consisting of 89% DMEM (Gibco, Billings, MT, USA) with 10% fetal bovine serum (FBS) (Gibco, Billings, MT, USA), 1% penicillin-streptomycin (Gibco, Billings, MT, USA), and 0.3% HEPES buffer solution (Sigma Aldrich, St. Louis, Missouri, USA). Subculturing was carried out when the cells reached 80–90% confluence by trypsinization using 1.0 mL of 0.05% (w/v) trypsin–0.53 mM EDTA solution. The cell suspension was centrifuged at 200×g for 10 minutes, and the cell pellet was resuspended with a complete growth medium and incubated at 37°C at a 5% CO_2 level.

Transfection using Lipofectamine 3000

Hepa1-6 wt cells were seeded in a 6-well plate at a density of 5×10^5 cells per well in 2 mL of complete growth medium. The cells were ready for the next treatment once they reached 80–90% confluence. The sgRNA sequence used in this step was the same as previously described [23]. However, the Donor DNA sequences differed, with the following sequence for Donor DNA mutated (Donor DNA mt) GAC GGC TCC GAT GAG TGG CCA CAG AAC TGC CAG GGC CGA GAC ACG GCC TCC AAA GGC GTT AGC AGC CCC TGC TCC TCC CTG GAG TTC CAC TGT GGT AGC AGT **TAG** TGT ATC CAT CGC AGC TGG GTC TGT GAC GGC GAG GCA GAC TGC AAG GAC AAG TCA GAT GAG GAG CAC TGC GCG GTG GCC ACC TGC CGA CCT GAT GAA TTC CAG.

The sgRNA, Cas9, and Donor DNA mt (2:1:0.04 ng/µL) were complexed prior to transfection into the cells using the transfecting agent Lipofectamine 3000 (ThermoFisher Scientific, Shanghai, China) [41-43]. A 2.07 µL Lipofectamine 3000 reagent was diluted with 100 µL Gibco Opti-MEM Reduced-Serum medium (ThermoFisher Scientific, Shanghai, China). An equal volume of Gibco Opti-MEM Reduced-Serum medium was added to the sgRNA, Cas9, and Donor DNA mt complex, followed by the addition of 1.38 µL P3000 reagent (ThermoFisher Scientific, Shanghai, China). The two solutions were mixed and incubated at room temperature for 15 minutes, of which a total of 200 µL of the solution was then added to Hepa1-6 wt cells that had been cultured in a 6-well plate. LDLR protein analysis was performed 72 hours post-transfection.

In vitro assay of Hepa1-6 *LDLR* mt

In vitro assays were used to investigate the changes in *LDLR* gene expression and LDLR protein levels in Hepa1-6 *LDLR* mt cells caused by LNP complex transfection in various formulas (**Table S4**). After 24 hours of incubation, cells from each formula were subcultured and evaluated visually using an optical microscope, followed by qRT-PCR and ELISA assays to measure *LDLR* gene expression and LDLR protein levels, respectively.

LDLR gene expression activity test

The RNA of Hepa1-6 *LDLR* mt cell was extracted using TRIzol LS reagent (ThermoFisher Scientific, Shanghai, China) according to standard procedure and then reverse transcribed into cDNA using the SensiFAST cDNA Synthesis Kit (Meridian Bioscience, Cincinnati, OH, USA) according to its protocol. Quantitative real-time reverse-transcription PCR (qRT-PCR) was analyzed with SYBR Green Real-Time PCR Master Mix (Toyobo, Osaka, Japan). The primers for

the wild-type *LDLR* gene were GTGTGATGGAGACCGAGATTG (forward) and CGGTTGGTGAAGAGCAGATAG (reverse). The *GAPDH* gene, used as a housekeeping gene, had the primers CCCCACACACATGCACTTACC (forward) and CCTAGTCCCAGGGCTTTGATT (reverse).

LDLR protein levels assay using ELISA

LDLR protein was extracted from approximately 1×10^6 cells/mL of Hepa1-6 *LDLR* mt cell, and the protein levels were quantified using the Mouse Low-Density Lipoprotein Receptor ELISA Kit (E0833Mo) (Bioassay Technology Laboratory, Shanghai, China). The measurement steps followed the manufacturer's established procedures.

Statistical analysis

All data were presented as mean with standard deviation (n=3). Optimization data related to the effect of homogenization time and speed were analyzed using the General Linear Model with a 2×2 factorial design. The uptake mechanism related to endocytosis and non-endocytosis pathways was analyzed using a paired t-test. Meanwhile, the gene expression was analyzed using one-way analysis of variance (ANOVA) followed by Tukey's post-hoc test. The other data associated with LNP characteristics and in vitro assays were analyzed using one-way ANOVA, followed by Dunnett's post-hoc test. All data have passed the normality test using Shapiro-Wilk. All analyses were conducted using Minitab 22 (Minitab LLC., State College, PA, USA).

Results

Production of LNP and characterizations

The LNP was formulated with different compositions (formula Fa to Fd) (**Table S1**), and the optimization was conducted to assess the impact of SOR on LNP characteristics. The results are presented in **Table 1**. The PSA results indicated that increasing the SOR caused a decrease in particle size. Fb until Fd formulas were statistically different compared to Fa formula ($p<0.05$). A correlation analysis approach was conducted to analyze the impact of SOR on PSA and PDI. Our data indicated that SOR strongly correlated with PSA according to the R-squared (R-Sq) value (**Figure 1A**). Meanwhile, the PDI values did not correlate with SOR (**Figure 1B**). The PDI values did not significantly change, ranging from 0.208±0.030 (Fc) to 0.314±0.060 (Fa). This PDI value indicated that all formulas had a suitable particle size uniformity because of its value ≤0.400. The contour plot graph visualizes the broader interaction of SOR values with PSA and PDI (**Figure 1C**). At SOR values between 0.2 and 0.6, the particle size was above 450 nm. Meanwhile, increasing the SOR to 1.0 caused the particle size to decrease to 350–400 nm. At higher SOR values (1.2–1.4), the particle size reached below 300 nm (**Figure 1C**). The PDI remained consistent with its value of ≤0.400 throughout these variations.

Table 1. Effect of surfactant to oil ratio (SOR) on particle size and polydispersity index (PDI) of lipid nanoparticle (LNP) produced.

Formula	Surfactant to oil ratio (SOR)	Particle size analysis (PSA) (nm)[a] Average±SD	Polydispersity index (PDI)[a] Average±SD
Fa	0.2	517.1±3.3	0.314±0.060
Fb	0.5	415.5±4.6*	0.301±0.089
Fc	0.9	327.8±2.1*	0.208±0.030
Fd	1.4	287.5±1.9*	0.248±0.039

[a]Data was analyzed using one-way ANOVA followed by Dunnett's post-hoc test. Data compared to Fa
*Statistically significant at $p<0.05$

Fd formula had the smallest particle size compared to the entire formula. However, the size was still quite large if the purpose of delivery is to be transfected into hepatocyte cells, where the particle size must be less than 150 nm. Therefore, particle size reduction was done using Homogenizer Ultra-turrax and Sonicator Probe with several treatment groups (**Table S2**). The relationship between the time and speed of the homogenizer with the particle size and PDI are presented in **Figure 2A**. F1 and F2 formulas had the same homogenization time of 2 minutes, while F3 and F4 were given homogenization treatment for 5 minutes. The homogenization speed

was varied between 5000 rpm (F1 and F3) and 7200 rpm (F2 and F4). The data showed that the particle size of each formula was as follows: F1 (288.6±5.3 nm), F2 (253.1±11.1 nm), F3 (170.6±2.1 nm), and F4 (144.8±6.7 nm). While the PDI values of F1, F2, F3 and F4 were 0.331±0.008, 0.341±0.038, 0.309±0.009 and 0.241±0.009, respectively. Based on the particle size curve against homogenizer time and speed, both lines were almost parallel and have a similar decreasing trend. In another part, both lines intersected in the PDI curve against the homogenizer's time and speed. Subsequently, optimization was conducted on F4 by varying the sonication duration utilizing the Sonicator Probe (**Figure 2B**). Sonication time was increased from 7.5 minutes (F4) to 10 minutes (F5), 16 minutes (F6), and 20 minutes (F7). Based on particle size measurements, the values obtained were 144.8±6.7 nm, 153.2±10.7 nm, 127.0±4.5 nm and 111.2±1.0 nm, respectively. At the same time, the PDI values produced were 0.241±0.009, 0.377±0.023, 0.293±0.049, and 0.253±0.040, consecutively.

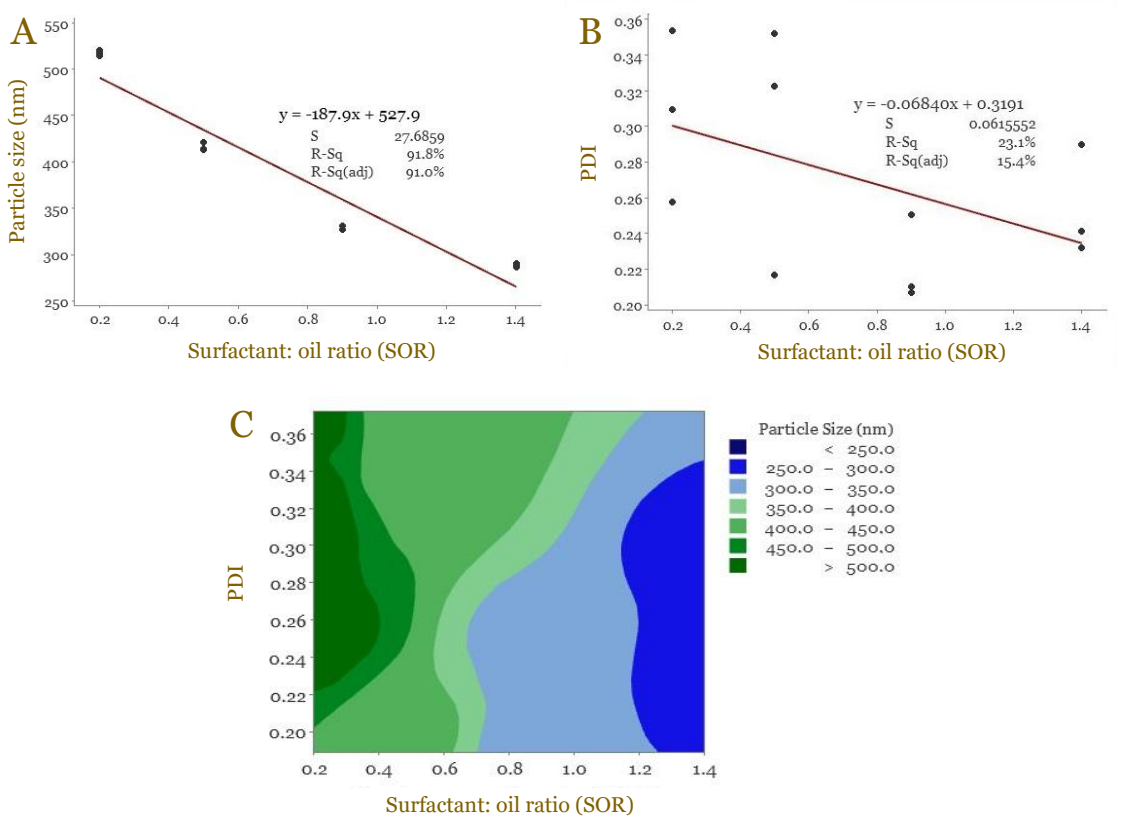

Figure 1. Effect of surfactant: oil ratio (SOR) on particle size analysis (PSA) and polydispersity index (PDI). (A) Correlation graph between SOR and PSA. (B) Correlation graph between SOR and PDI. (C) The contour plot diagram illustrates a comparative analysis of the increase in SOR concerning PSA and PDI.

Furthermore, DSPE-PEG$_{2000}$-NH$_2$ and PEI were integrated into the F7 (**Table S3**). Incorporating DSPE-PEG$_{2000}$-NH$_2$ into the LNP formulation (F8) resulted in a minor particle size and PDI elevation, measuring 113.6±0.7 nm and 0.267±0.038, respectively. The most significant particle size and PDI compared to F7 were observed in F9, which were 118.6±0.8 nm and 0.347±0.030, respectively (**Figure 3A**). The zeta potential of F9 was 7.5±0.7 mV, where the DSPE-PEG$_{2000}$-NH$_2$ and PEI significantly increased the positive charge on the nanoparticle surface compared with F7 (3.7±0.8 mV). Meanwhile, the zeta potential of F7 was not significant compared to F8 (4.2±0.5 mV) (**Figure 3B**). The F9 formula component constituted the basis for the development of LNP Blank.

Following this, FTIR spectroscopy was used to confirm the functionalization and components of the LNP Blank (**Figure 3C**). The LNP Blank had several significant peaks, notably 3268 cm^{-1}, corresponding to the N-H stretching vibrations characteristic of PEI's primary and secondary amino groups. Furthermore, peaks located at 2918 cm^{-1} and 2851 cm^{-1} represented the symmetric and asymmetric C-H stretching vibrations of the aliphatic chain. Each peak reflected

the structural characteristics of DOTAP, DSPE-PEG_{2000}-NH_2, and PEI. An additional peak was observed at 1736 cm^{-1}, indicating the presence of a carbonyl group (C=O) from the ester group from DOTAP and DSPE-PEG_{2000}-NH_2. The peak at 1457 cm^{-1} represented the C-H bending vibration. This latter peak was also identified in DOTAP, DSPE-PEG_{2000}-NH_2 and PEI.

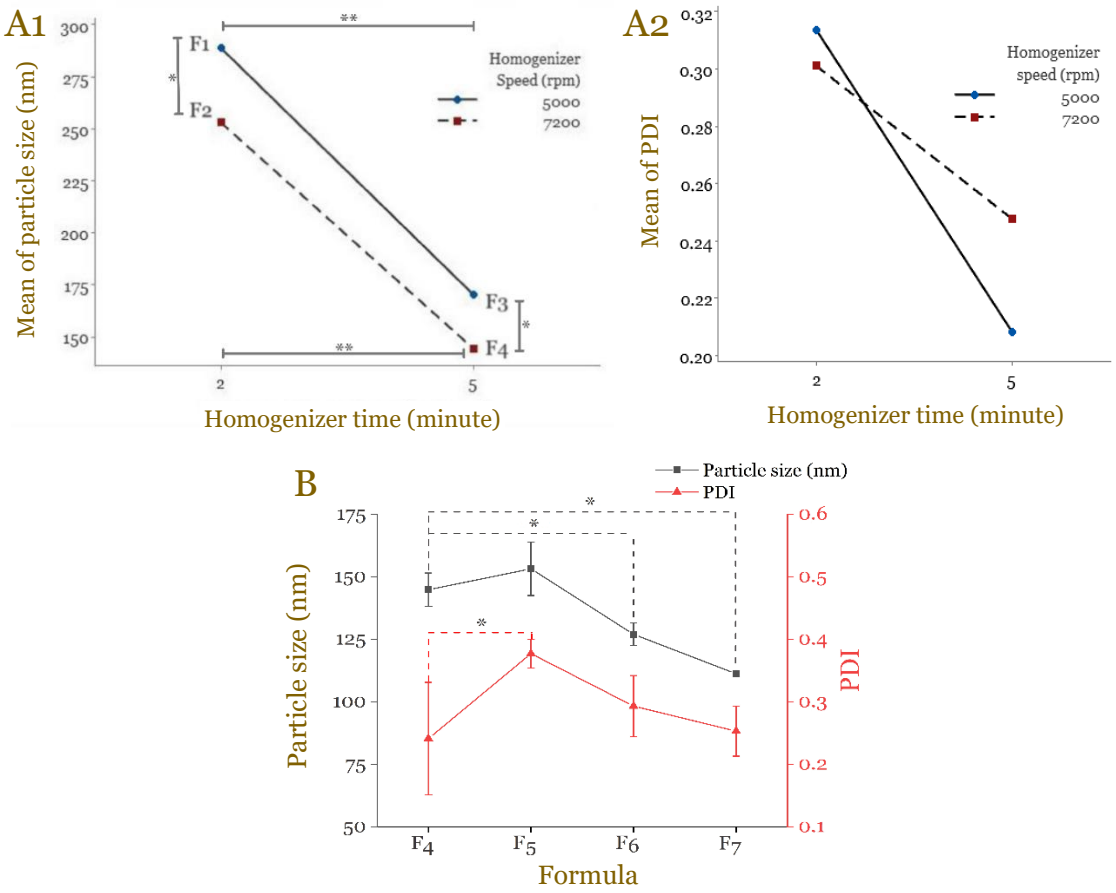

Figure 2. Graphic analysis of particle size analysis (PSA) and polydispersity index (PDI) measurement results in F1 to F7. (A) Analysis of PSA and PDI results on F1-F4. Data was analyzed using General Linear Model with a 2×2 factorial design. (B) PSA and PDI analysis on F4-F7. Data was analyzed using one-way ANOVA followed by Dunnett's post-hoc test. Data compared to F4. Statistically significant at $^{*}p<0.05$; $^{**}p<0.01$.

The morphology of LNP Blank was observed using a TEM (**Figure 3D**). The nanoparticles predominantly exhibited a spherical morphology. However, some particles underwent agglomeration. The histogram depicting particle size distribution indicated adherence to a normal (Gaussian) distribution, with a size range extending from 0 to 200 nm. A significant proportion of particles was measured to fall within the 50 to 150 nm range. This result was supported by the entrapment efficiency (% EE) assay. LNP Blank had a % EE of 88.01±0.87%.

Viability testing with the MTT assay was used to evaluate the effects of various concentrations of LNP Blank on Hepa1-6 wt cells (**Figure 4**). The results of the MTT assay indicated that LNP Blank concentrations of 3.6 mM and 7.2 mM resulted in Hepa1-6 wt cell viability levels of 95.05±2.29% and 88.99±4.37%, respectively. These findings were insignificant when contrasted with the negative control (untreated group). The application of LNP Blank at concentrations ranging from 14.4 mM to 230.4 mM demonstrated a significant induction of cell death compared to the untreated group ($p<0.01$). The cell viability values were as follows: 82.06±4.7%, 52.73±9.07, 31.8±3.96%, 24.19±7.63%, and 15.51±2.31%. Hepa1-6 wt cells transfected with Tween 20 (5%) as a positive control showed 14.27±5.16% cell viability. Based on the data series, the IC_{50} value obtained was 27.7 mM.

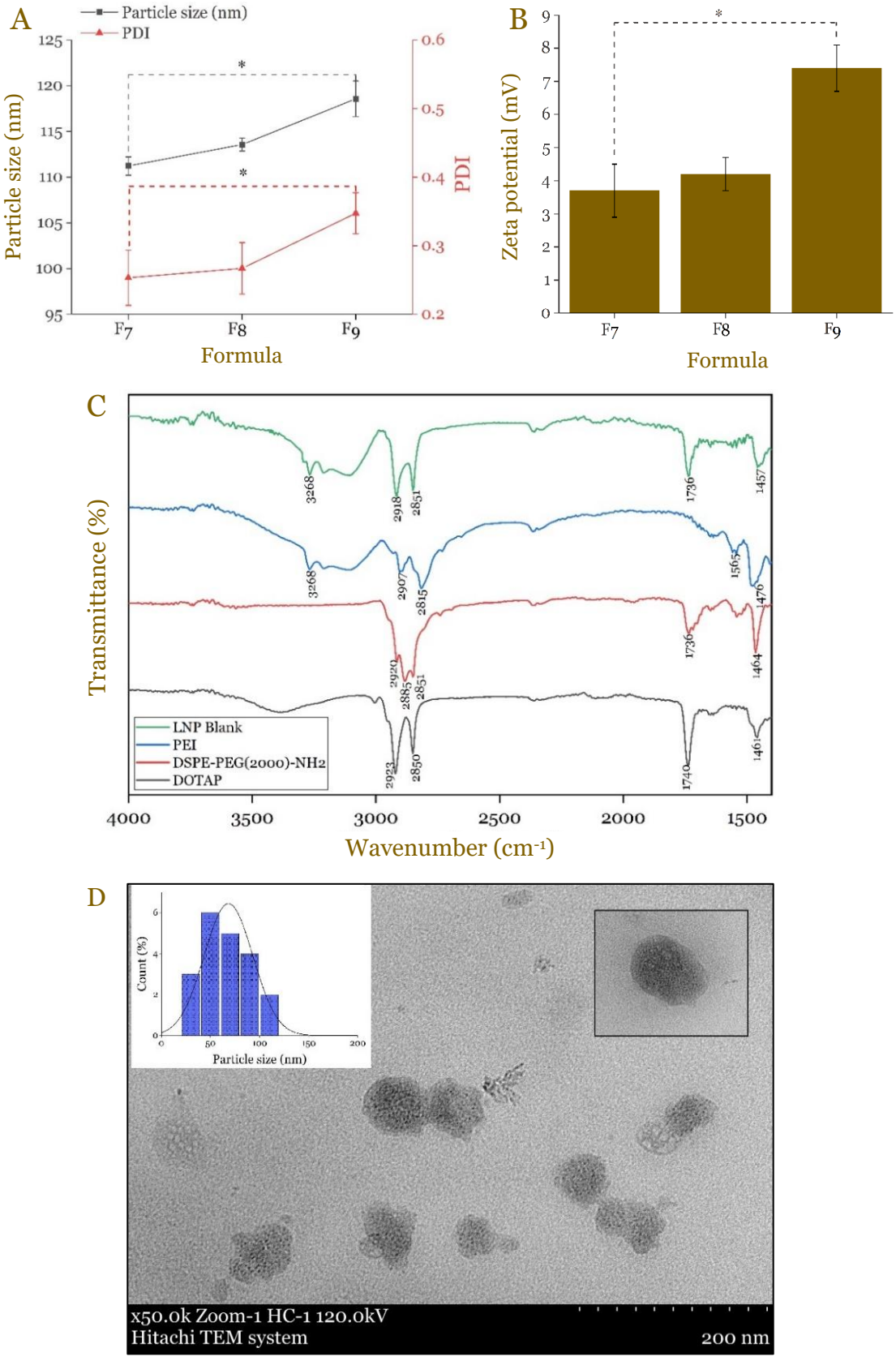

Figure 3. Determination of lipid nanoparticles (LNP). (A) Particle size analysis (PSA) and polydispersity index (PDI) values of F7-F9. Data was analyzed using one-way ANOVA followed by Dunnett's post-hoc test. Data compared to F7. (B) Zeta potential analysis of F7-F9. Data was analyzed using one-way ANOVA followed by Dunnett's post-hoc test. Data compared to F7. (C) FTIR analysis of F9. (D) Transmission electron microscope (TEM) of F9. The inset shows a particle size distribution graph of LNP. *Statistically significant at $p<0.05$.

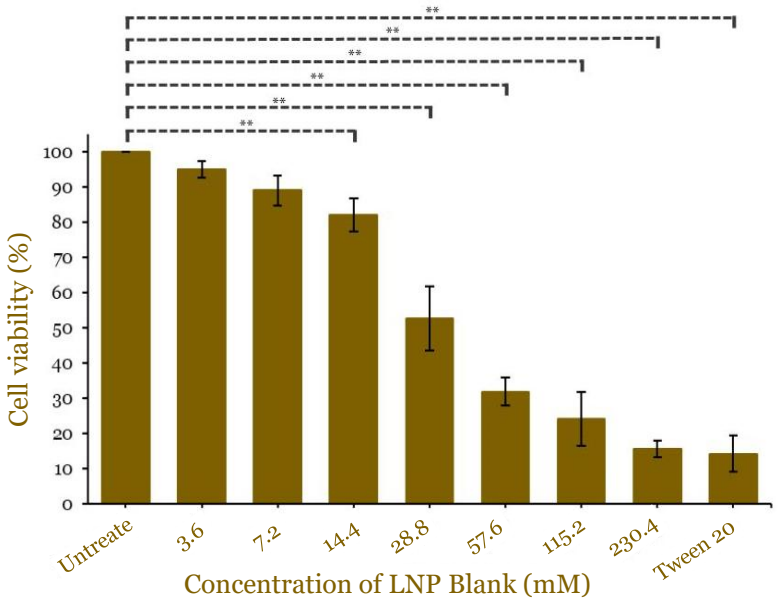

Figure 4. Viability test results of lipid nanoparticles (LNP) Blank (F9 formula) on Hepa1-6 wt cells. Data was analyzed using one-way ANOVA followed by Dunnett's post-hoc test. Data compared to the untreated group. **Statistically significant at $p<0.01$.

The ability of LNP Blank to penetrate the Hepa1-6 wt cells can be observed through the cellular internalization assay. Based on quantitative data, the non-endocytosis pathway demonstrated a fluorescence intensity of 122.22±53.10, significantly different from the endocytosis pathway, which exhibits a fluorescence intensity of 1058.73±67.64 ($p<0.001$). (**Figure 5A** and **5C**). Subsequent assessment was carried out by observing the endocytosis pathway used by LNP Blank in penetrating Hepa1-6 wt cells (**Figure 5B** and **5D**). Untreated cells exhibited a maximum cellular uptake of 100±0.00%. The introduction of 0.4 M sucrose as an inhibitor of CME resulted in a substantial reduction in uptake, measuring at 10.34±2.31% ($p<0.0001$). Similar results were observed with 0.1 mM amiloride and 5 µg/mL filipin, which also induced significant decreases in cellular uptake to 66.62±13.07% ($p<0.0001$) and 73.45±11.70% ($p<0.0001$), respectively. All experimental groups were compared to the untreated group cells.

Production of Hepa1-6 LDLR mt cell for in vitro model

The efficiency of sgRNA and Donor DNA mt in producing Hepa1-6 *LDLR* mt cells was determined by estimating the frequency of occurring mutations. **Figure 6A** indicates the precision of the editing process. The total efficiency reached 49.2% with a value of $R^2=1$, indicating high precision in the editing process. The insertion process was seen at 0 (zero) position with a percentage of 50.7%, while no significant deletions were detected. Moreover, **Figure 6B** illustrates that the efficiency of homology-directed repair (HDR) attained a notable 49%.

Production of LNP complex

LNP Blank was mixed with sgRNA, Cas9, and Donor DNA wt to produce the LNP complex (**Table S4**). Based on the N/P ratio, the ratio used was 4.5:1. The particle size and PDI of the LNP complex were measured for each formula (**Figure 7**). The particle size of LNP Blank and LNP complex from F-LNP1 to F-LNP8 were 118.6±0.8 nm, 118.1±1.0 nm, 118.8±0.8 nm, 119.3±0.9 nm, 119.5±0.6 nm, 120.3±0.8 nm, 121.2±0.7 nm, 122.1±1.1 nm, and 122.5±0.9 nm, respectively. Meanwhile, the PDI values were 0.347±0.030, 0.217±0.048, 0.248±0.030, 0.268±0.039, 0.301±0.087, 0.327±0.042, 0.333±0.098, 0.318±0.077, and 0.310±0.095, successively. The particle size of F-LNP6, F-LNP7 and F-LNP8 experienced a significant increase compared to LNP Blank ($p<0.05$). However, the PDI value concluded that all LNP complex formulas were insignificant to LNP Blank.

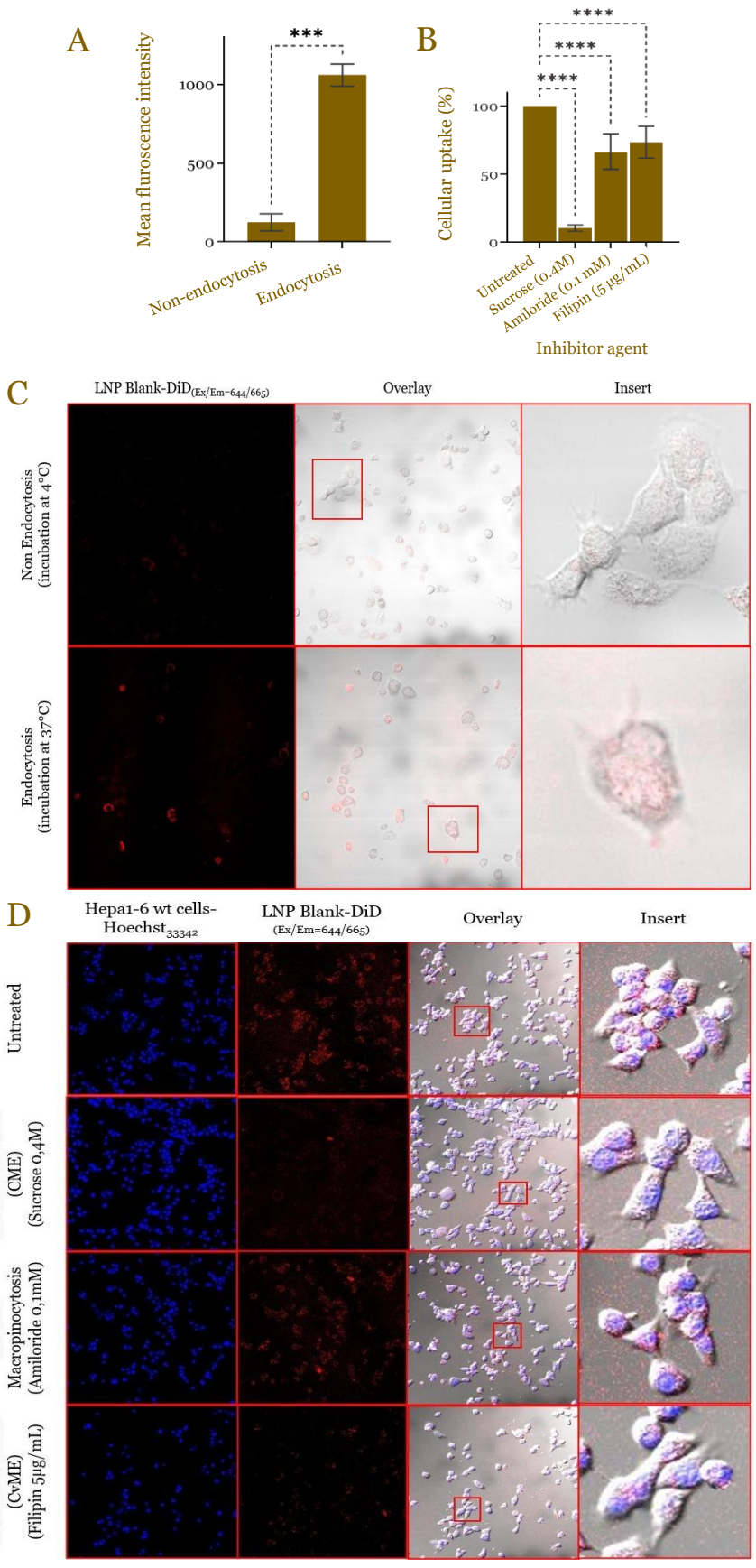

Figure 5. Cellular uptake assay of lipid nanoparticles (LNP) in Hepa1-6 wt cells. (A and C) Endocytosis and non-endocytosis test with the graph of fluorescence intensity values. Data was analyzed using paired t-test. (B and D) Clathrin-mediated endocytosis (CME), macropinocytosis, and caveolae-mediated endocytosis (CvME) with the graph of cellular uptake. Data was analyzed using one-way ANOVA followed by Dunnett's post-hoc test. Statistically significant at $^{***}p<0.001$; $^{****}p<0.0001$.

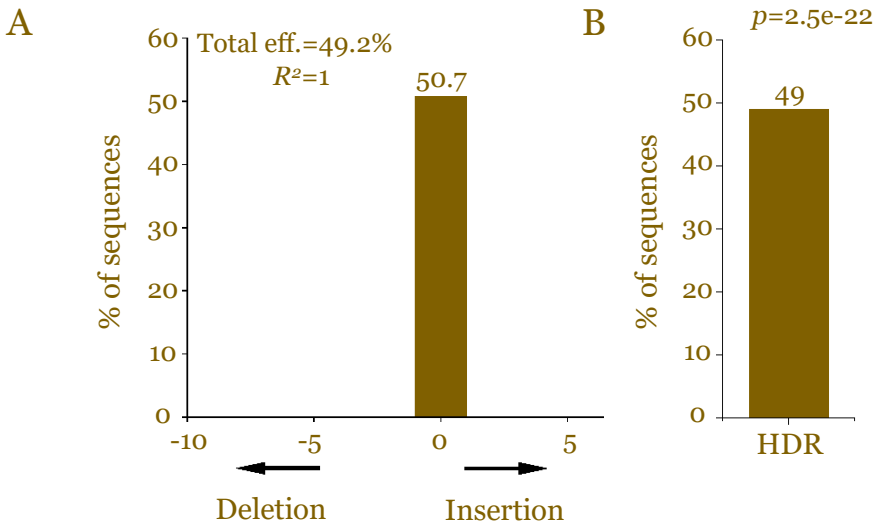

Figure 6. TIDER analysis of sgRNA and Donor DNA mt design. (A) The efficiency of the editing process. (B) The efficiency of homology-direct repair (HDR).

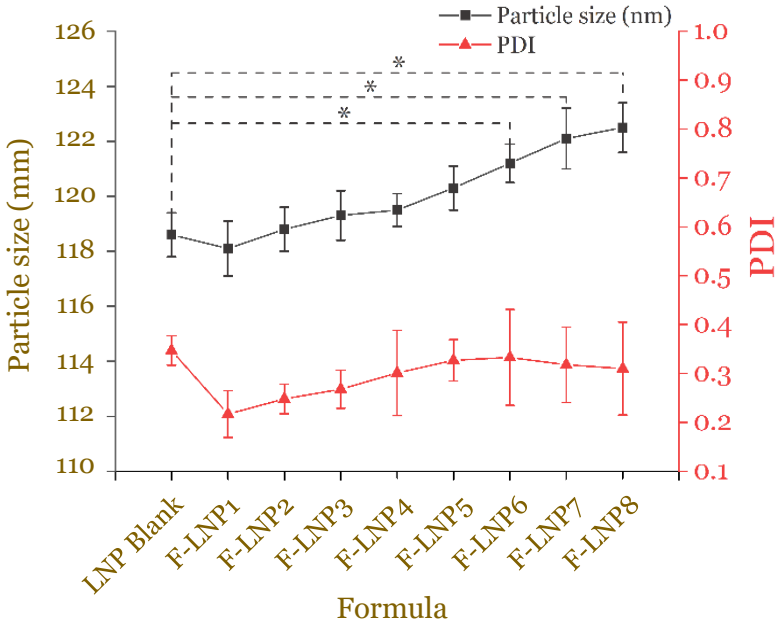

Figure 7. Data on particle size analysis (PSA) and polydispersity index (PDI) measurements from various lipid nanoparticles (LNP) formulations. Data was analyzed using one-way ANOVA followed by Dunnett's post-hoc test. * Statistically significant at $p<0.05$.

In vitro assay

The F-LNP1 to F-LNP8 were then transfected into Hepa1-6 *LDLR* mt cells and incubated for 24 hours. Cells were then subcultured for observations regarding cell morphology, *LDLR* gene expression via qRT-PCR, and LDLR protein levels using an ELISA kit. Based on cell morphology observed using an optical microscope at the same magnification, there were differences in growth cells (**Figure 8**). Hepa1-6 *LDLR* mt cells transfected by F-LNP1 to F-LNP6 (**Figures 8C-8H**) appeared to grow well, as shown as Hepa1-6 *LDLR* mt cells (**Figure 8B**). Different results appeared in Hepa1-6 *LDLR* mt cells transfected by F-LNP7 to F-LNP8 (**Figures 8I-8J**) of which the cells were dead, characterized by cell lysis. This indicated that F-LNP7 and F-LNP8 influence the cell growth. Based on this, these formulas (F-LNP7 and F-LNP8) were eliminated from the further observation and study.

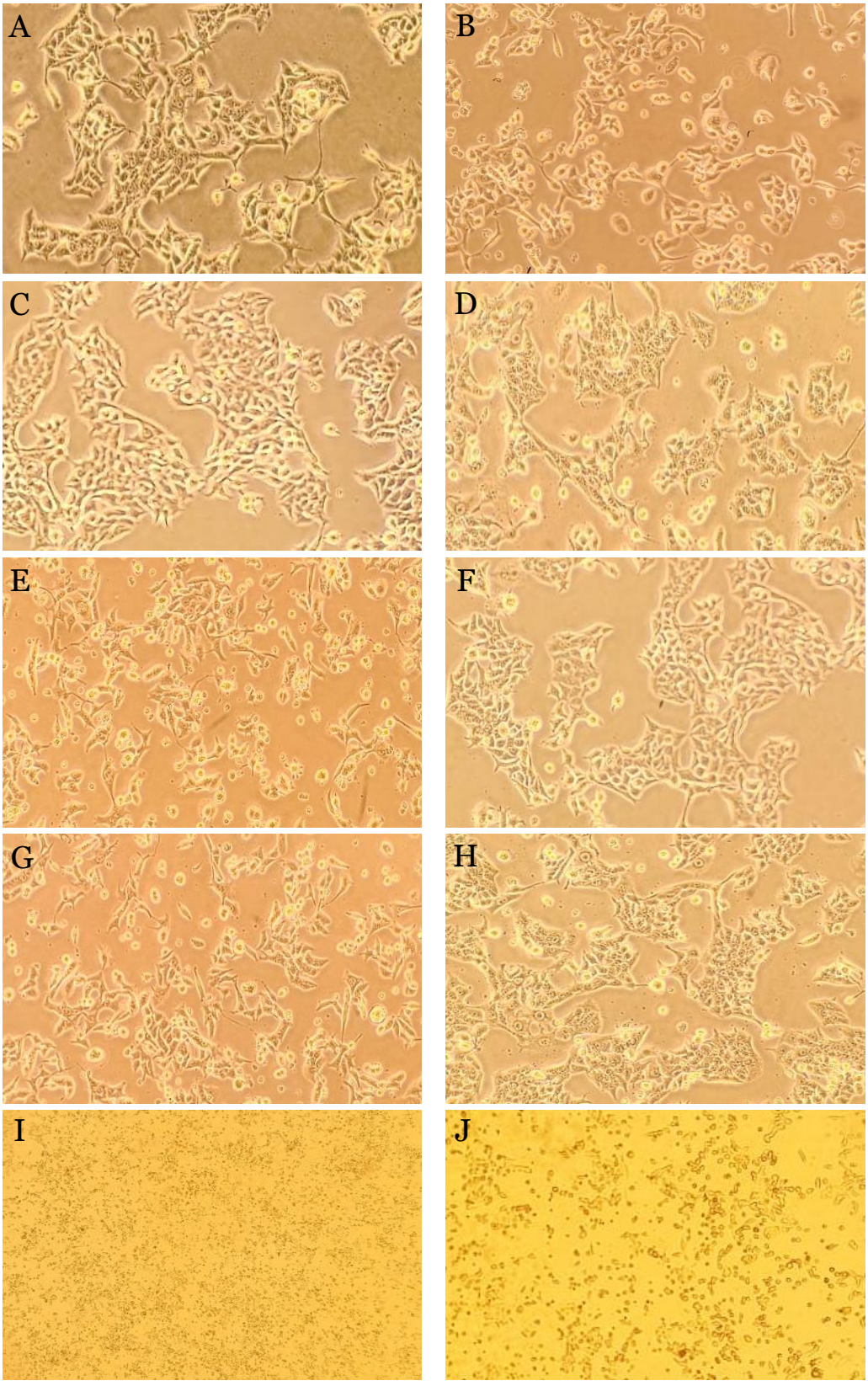

Figure 8. Image of cells after 24 hours of transfection with LNP-CRISPR/Cas9-Donor DNA wt. (A) Hepa1-6 wt as a controlled cell; (B) Hepa1-6 *LDLR* mt cells; (C) to (J) Hepa1-6 *LDLR* mt cells transfected by F-LNP1 to F-LNP8.

The LDLR protein levels were carried out 24 hours after transfection. Then continue on the 4th, 7th, and 10th days (**Figure 9A**). On the initial day of observation, the LDLR protein did not significantly alter. The LDLR protein levels of Hepa1-6 *LDLR* mt, F-LNP1, F-LNP2, F-LNP3, F-LNP4, F-LNP5, and F-LNP6 were 9.68±0.40 ng/mL, 10.10±0.41 ng/mL, 10.15±0.37 ng/mL,

10.61±0.35 ng/mL, 11.17±0.42 ng/mL, 11.19±0.52 ng/mL, and 11.29±0.46 ng/mL, respectively. Meanwhile, on the 4th day, the LDLR protein levels were consecutively 9.88±0.35 ng/mL, 10.67±0.46 ng/mL, 10.75±0.41 ng/mL, 11.09±0.37 ng/mL, 12.34±0.31 ng/mL, 12.95±0.25 ng/mL, and 13.14±0.35 ng/mL. Significant changes occurred in F-LNP5 and F-LNP6 compared to Hepa1-6 *LDLR* mt as a control (p<0.01).

On the 7th day, the LDLR protein levels were 9.77±0.42 ng/mL, 11.32±0.21 ng/mL, 11.39±0.29 ng/mL, 12.67±0.28 ng/mL, 12.58±0.27 ng/mL, 13.18±0.49 ng/mL, and 13.63±0.54 ng/mL. On day 7, besides F-LNP5 and F-LNP6, F-LNP4 also showed significant differences from control (p<0.01). At the 10th day, the LDLR protein levels were 9.97±0.39 ng/mL, 11.84±0.24 ng/mL, 11.93±0.22 ng/mL, 13.02±0.56 ng/mL, 13.46±0.48 ng/mL, 13.56±0.40 ng/mL, and 13.52±0.22 ng/mL. The F-LNP3, F-LNP4, F-LNP5, and F-LNP6 showed a significantly different result with the control (p<0.01).

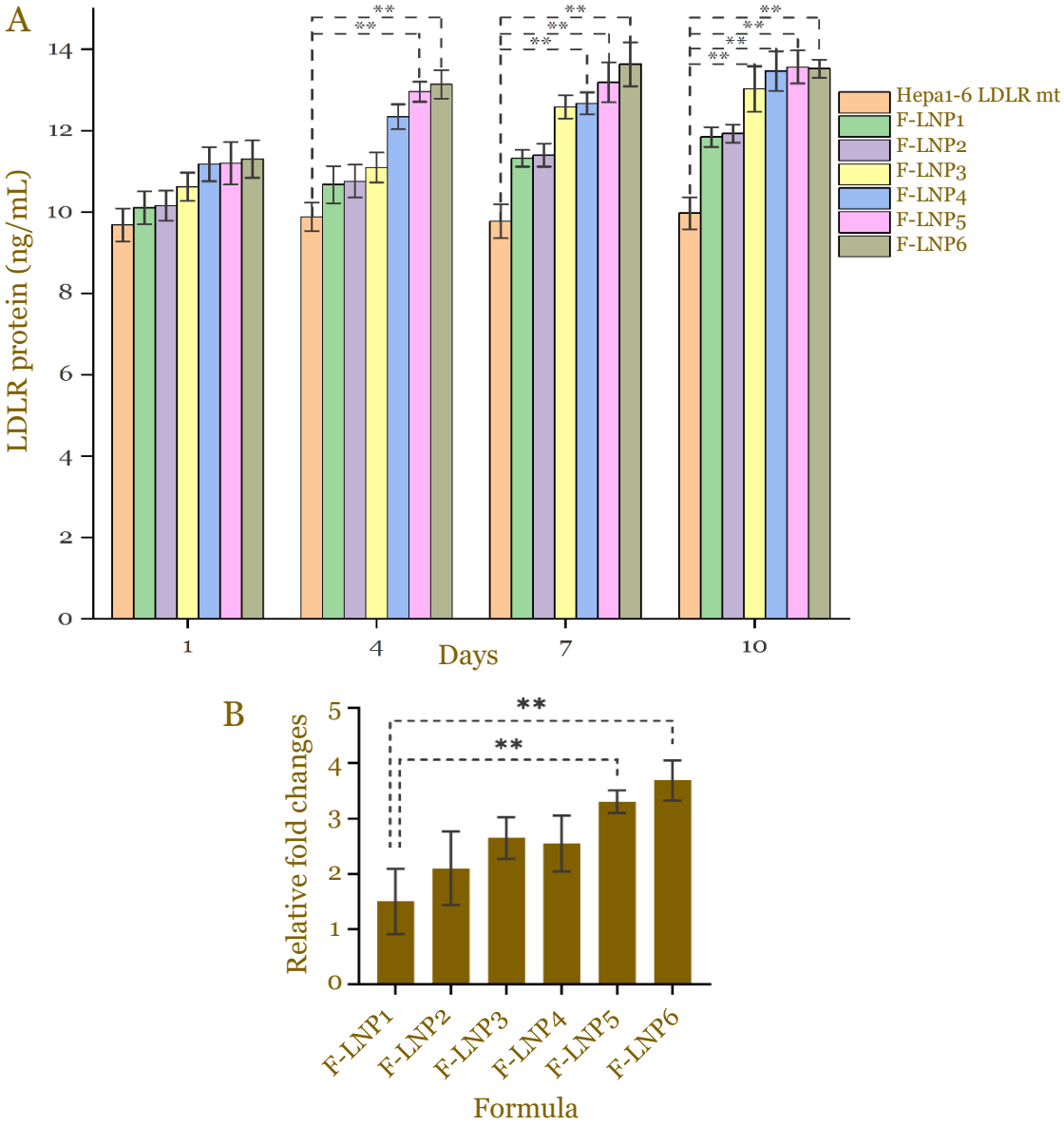

Figure 9. Data from the measurement of *LDLR* gene and protein expression. (A) Protein *LDLR* levels from various formulas on the 1st to 10th day of measurement. Data was analyzed using one-way ANOVA followed by Dunnett's post-hoc test. Data compared to Hepa1-6 *LDLR* mt group. (B) *LDLR* gene expression in various F-LNP formulas. Data was analyzed using one-way ANOVA followed by Tukey's post-hoc test. **Statistically significant at p<0.01.

The *LDLR* gene expression was assessed by qRT-PCR (**Figure 9B**). The relative fold changes of the *LDLR* gene expression of F-LNP1, F-LNP2, F-LNP3, F-LNP4, F-LNP5, and F-

LNP6 were 1.5±0.6, 2.1±0.7, 2.7±0.4, 2.6±0.5, 3.3±0.2, and 3.7±0.4, respectively. F-LNP1 differed significantly from F-LNP5 and F-LNP6 (p<0.01).

Discussion

Developing effective and safe drug delivery systems is critical to advancing gene therapy, particularly for CRISPR/Cas9 technology. This study presented a comprehensive analysis of the development and optimization of LNP systems, with special emphasis on formulation parameters that affect their physicochemical characteristics and cellular interactions. The LNP system consists of squalene as a lipid base in pharmaceutical preparations, glyceryl trimyristate as an emulsifier, DOTAP as a cationic lipid to facilitate gene delivery, and a combination of Span 60 and Tween 80 as a non-ionic surfactant for nanoparticle stabilization (**Table S1**). Optimization of the SOR became the study's initial focus, given its significant influence on particle size and distribution (**Table 1**) [44-46]. Regression analysis showed that an increase in SOR caused a decrease in the particle size of LNP with regression equation y=−187.9x+527.9 and R-Sq=0.918 (**Figure 1A**). The R-Sq value approaching 1.0 indicates that the changes in the SOR show a strong correlation to particle size. This decrease in particle size could occur through several mechanisms, such as increased micellar nucleation efficiency, forming a protective layer that prevents aggregation, and increased steric stabilization of the system because of the combination of surfactant and oil [18]. However, the SOR did not change the particle size distribution (**Figure 1B**). The PDI value in each formula was below 0.400, which showed that the system was uniformly sized (monodisperse) [44-46]. From all over formulas, Fd had the characteristics of the smallest particle size with a homogeneous population of nanoparticles.

The optimization in the manufacturing process was carried out through homogenization using Homogenizer Ultra-turrax (**Table S2**). The General Linear Model analysis with a factorial design of 2×2 confirmed the significant influence of homogenization speed and time on particle characteristics (**Figure 2A**). Homogenizer Ultra-turrax with a process time of 2 minutes (F1 vs F2) and 5 minutes (F3 vs F4), each comparison showed a significant decrease in particle size along with increasing speed of the homogenizer (p<0.05). The same results were also demonstrated when comparing 2 formulas with the same speed (F1 vs F3 and F2 vs F4), where increasing homogenization time also caused a decrease in particle size (p<0.01). Considering the relationship between particle size versus the homogenizer's time and speed, the two lines were approximately parallel and exhibited a similar decline. This indicated that the homogenizer's time and speed work independently to affect particle size. However, the effect of homogenization time and speed did not significantly impact the PDI value. The resultant curve likewise evidenced the corresponding outcomes. Both lines intersect on the PDI curve against the homogenizer's time and speed. This showed that increasing the time and speed of homogenization did not always impact increasing the PDI value. The homogenization time showed a more dominant influence on particle size reduction, indicating the importance of the duration of exposure to shear forces [33,47]. The F4 formula, which combined high speed with longer homogenization time, produced an optimal combination of particle size reduction. Previous studies also found the same results [47].

Advanced optimization was performed using a Sonicator Probe with variations in sonication time (**Table S2**). There was a significant decrease in particle size during the sonication process (**Figure 2B**). The particle size of F4 significantly differed from that of F6 and F7 (p<0.05). In contrast, F5 did not significantly differ from F4. This was due to temporary particle reaggregation [48,49]. Conversely, the PDI value showed that F4 significantly differed from F5 (p<0.05) but yielded insignificant results for F6 and F7. Nevertheless, this value remained within acceptable limits, indicating a uniform particle size distribution. Formula F7 achieved an optimal balance between particle size reduction and size distribution. Previous studies revealed that the sonication process was linked to particle reorganization dynamics that influence the particle size reduction of LNPs [49-51].

Modification of the nanoparticle surface was carried out by the addition of DSPE-PEG$_{2000}$-NH$_2$ and PEI (**Table S3**). PEGylation improves steric stability, provides a "stealth" effect on the body's defense system, and prevents opsonization [21,52,53]. Meanwhile, PEI contributes to increased cellular transfection efficiency through the proton sponge effect and increased surface

positive charge [53-55]. This modification resulted in significant changes of the LNP characteristics (**Figure 3A**). The F9 formulation demonstrated substantial alterations in particle size and PDI values compared to F7 ($p<0.05$). In contrast, F8 and F7 did not exhibit significant. Despite that, these characteristics are still within the acceptable range for nanoparticle drug delivery systems targeting liver cells: particle size ≤150 nm and PDI≤0.400 [11-14]. Characterization of zeta potential showed a significant increase in F9 compared to F7 ($p<0.05$) (**Figure 3B**). PEI in the formula is known to have a high buffering capacity due to the presence of primary, secondary, and tertiary amino groups that can be protonated, thus providing a higher positive charge density on the nanoparticle surface [56-59]. The stability of LNP depends not only on electrostatic repulsion but also on steric stabilization provided by the PEG chain. Combining electrostatic and steric stabilization can produce a good LNP system [60,61]. This F9 formulation was then referred to LNP Blank. Molecular interactions between components in LNP Blank were observed through FTIR spectroscopic analysis (**Figure 3C**). This interaction is related to the ability of LNP Blank to maintain the structure of nanoparticles [51,62]. Based on observations, the components that make up the formula were still detected in LNP Blank. Moreover, morphological analysis conducted using TEM indicated that LNP Blank demonstrated a spherical morphology. The observed size distribution pattern demonstrated a uniform nucleation process and particle growth, which favorably affect the LNP's entrapment efficiency and stability [63-65]. This outcome corroborated the successful preparation of the developed LNP Blank.

Before conducting in vitro testing concerning the efficacy of lipid nanoparticles on target cells, it is important to evaluate the effects of LNP on cell viability and metabolic activity, as assessed through MTT assay (**Figure 4**). Applying LNP Blank at concentrations of 3.6 mM and 7.2 mM was safe, as these concentrations did not induce significant cell death compared to the untreated group. The determined IC_{50} value of 27.7 mM indicated that, at this concentration, 50% of the Hepa1-6 wt cell population was dead. Accordingly, utilizing a maximum LNP Blank concentration of 7.2 mM is considered a safe concentration as a delivery system for hepatocyte cells. This can be attributed to the amphiphilic properties of lipid components that allow for proper interaction with cell membranes without interfering with cell integrity [66]. On the other hand, increasing LNP concentration can also decrease cell viability. This can be caused by disruption of cell membranes, oxidative stress, or activation of apoptosis pathways [67,68]. The Tween 20 (5%) solution, as a positive control, is related to its toxicity mechanism to the cells, where cell membrane damage due to Tween 20 occurs through dissolving membrane lipids [69]. Tween 20 toxicity data can be a reference in determining the upper limit of undesirable toxicity levels and help optimize surfactant concentrations in the LNP formula [70-72].

Investigation of cellular uptake mechanisms using fluorescence microscopy and inhibitor studies confirmed endocytosis as the main pathway. This 10-fold difference in fluorescence intensity between non-endocytosis and endocytosis confirmed that endocytosis was the main pathway in the internalization of LNP Blank into Hepa1-6 wt cells ($p<0.001$). A comprehensive investigation concerning the endocytosis pathway utilized by the LNP Blank, conducted with specific endocytosis pathway inhibitors, demonstrated that CME dominated cellular internalization compared to other mechanisms (**Figure 5**). The fluorescence distribution pattern showed accumulation in the cytoplasmic region and localization in the perinuclear region, indicating efficient intracellular trafficking [73-75]. The success of internalization was supported by the optimal particle size (≤150 nm) as well as the presence of surface modifications that increase interaction with cell membranes, and the proton sponge effect of DSPE-PEG_{2000}-NH_2 and PEI [61,74,76].

In vitro testing was conducted using Hepa1-6 *LDLR* mt cells. These cells represent cells that have familial hypercholesterolemia [42]. However, before that, the production of these mutated cells must be carried out. The process commenced with designing and analyzing the effectiveness of sgRNA and Donor DNA mt through TIDER analysis [30]. The results showed that the genome editing efficiency reached 49.2%, where 50.7% occurred through an insertion with no detection of the deletion process (**Figure 6A**). Furthermore, a more specific analysis was carried out regarding the gene editing mechanism from the insertion process. Based on the TIDER analysis, 49% of the gene editing process by insertion occurred through the homology-direct repair (HDR) mechanism (**Figure 6B**). This is a remarkable achievement considering that HDR efficiency

above 40% indicates optimal results for genome editing applications in mammalian cells [30,77]. These results indicated that the sgRNA and Donor DNA mt have been well designed, as evidenced by the results of TIDER analysis. Furthermore, the process of forming Hepa1-6 cells mutated in the *LDLR* gene was carried out by transfecting these components with the help of the transfecting agent Lipofectamine 3000. The effectiveness of this process was observed by measuring the LDLR protein levels from Hepa1-6 wt cells compared to Hepa1-6 *LDLR* mt cells. The assay showed that the LDLR protein levels from Hepa1-6 wt cells to Hepa1-6 *LDLR* mt cells decreased significantly, 13.75±0.30 ng/mL and 9.68±0.40 ng/mL, respectively ($p<0.01$). These results confirmed that the production of Hepa1-6 *LDLR* mt cells as a cell model of familial hypercholesterolemia has been valid for subsequent in vitro studies.

Before in vitro testing, LNP Blank was complexed with genetic material containing sgRNA, Cas9, and Donor DNA wt (**Table S4**). Based on the calculation of the N/P ratio which describes the comparison between the positive charge of cationic lipids (N) and the negative charge of nucleic acids (P), resulting in a value of 4.5: 1. This value is related to the efficiency of the complexity between lipids and nucleic acids and the transfection efficiency of LNPs [78]. Based on previous studies, the optimal N/P ratio for LNP-based gene delivery systems ranges from 3:1 to 8:1 [79-81]. Moreover, the LNP complex was measured by particle size and PDI (**Figure 7**). The results showed a correlation between the variation in sgRNA and Donor DNA wt concentrations on the increase in particle size, with significant characteristic changes observed in F-LNP6 to F-LNP8 compared to LNP Blank, especially when the concentration of Donor DNA wt exceeded 0.04 ng/µL. Electrostatic interactions between charged components and the process of reorganization of nanoparticle structures play an important role in these conditions [29,82,83]. Despite the increase in particle size, the size was still below 150 nm with a PDI below 0.40. This is important to maintain because it is related to the target cells of this LNP, which is to go to hepatocyte cells [16-18]. The F-LNP1 to F-LNP8 formulas were then transfected into Hepa1-6 *LDLR* mt cells to evaluate the effectiveness of genetic editing.

The in vitro assay was carried out on the formulation of F-LNP1 to F-LNP8 transfected into Hepa1-6 *LDLR* mt cells. Morphological observations using an optical microscope show the characteristics of hepatocyte cells with a polygonal shape that form compact colonies (**Figure 8**). F-LNP1 to F-LNP6 exhibited uniform cell density with intact cell membranes and clear cytoplasm, indicating good biocompatibility without cytotoxic effects. However, in F-LNP7 and F-LNP8, cell death occurred due to excessive concentration of Donor DNA wt, which triggered cellular stress. Previous studies have suggested that excessive concentrations of Donor DNA in gene editing via the HDR mechanism can be considered a foreign object by the cells, that could cause cellular stress, leading to the death of cells [27,84]. Therefore, both formulas were excluded from the test.

The LDLR protein levels and gene expression analysis showed a consistent trend compared to the Hepa1-6 *LDLR* mt groups as a control. A significant rise in LDLR protein levels on the 4th day, especially in F-LNP5 and F-LNP6, which contain Donor DNA wt 0.04 ng/µL, was observed compared to the control ($p<0.01$) (**Figure 9A**). This indicated that the gene editing process in Hepa1-6 *LDLR* mt cells has occurred. Delivering LNPs to target cells can take 4–6 hours. Furthermore, LNPs struggle to penetrate the nucleus, a process that can take 12–24 hours. New gene expression appears 24–48 hours later [85-87]. This explains why a significant increase in LDLR protein levels was detected on day 4, which was also observed in LDLR gene expression by qRT-PCR (**Figure 9B**). In addition, the sufficient concentration of Donor DNA wt in the formulation also impacts the speed of gene editing and this is in line with previous research [82,88]. Based on the data, observations on the third day have begun to show an increase in LDLR protein levels compared to controls. Transfection of genetic material into Hepa1-6 *LDLR* mt cells, with the LNP as a delivery system, has caused the gene editing process to run optimally. This indicated that there has been genetic improvement on these cells. The increase in LDLR protein levels indicated that the mutated cells have gradually healed and formed revertant cells with characteristics resembling normal cells. The concentration of Donor DNA wt of 0.04 ng/µL was the optimal concentration in this study. The availability of sgRNA also impacts the efficiency of gene editing. This is related to the mechanism of sgRNA, where it will direct the Cas9 protein towards the target DNA sequence for the cutting process to form a double-strand break (DSB) [9,13,89-91]. Therefore, the concentration of sgRNA and Donor DNA is an important parameter

that must be considered in genetic editing. In this study, the ratio of sgRNA: Cas9: Donor DNA wt (1:1:0.04) was proven to provide optimal gene editing results, with significant increases in gene expression and LDLR protein levels seen on day 4 post-transfection. These results confirm the potential formulation of LNP as an effective genetic material delivery system for treating familial hypercholesterolemia.

Even though the results were promising, this study has some limitations. Validation through in vivo experiments is needed to confirm the efficacy and safety of the LNP formula. Several in vivo assays, such as the evaluation of blood circulation and biodistribution test, must be done to advance this therapeutic approach. It also needs to ensure long-term toxicity and biocompatibility. Adjusting these aspects will optimize the broader clinical use of LNP formulas for gene therapy.

Conclusion

By gradually modifying the LNP formulation process, LNPs that met the physicochemical characteristics required for targeted delivery to hepatocytes were successfully produced. The internalization process occurred via the CME pathway. LNPs were then complexed with sgRNA, Cas9, and Donor DNA wt to evaluate their effectiveness in delivering genetic material for the treatment of familial hypercholesterolemia using a gene therapy approach. The study was conducted through in vitro assays using Hepa1-6 LDLR mt cells as a model for familial hypercholesterolemia conditions. LNP complexes with a genetic material ratio of sgRNA:Cas9:Donor DNA wt (1:1:0.04) demonstrated significant therapeutic potential in the familial hypercholesterolemia model, as evidenced by the refunctionalization of the *LDLR* gene, which had previously lost its function. By the fourth day post-transfection, an increase in *LDLR* gene expression and LDLR protein production was observed, approaching levels seen in normal cells. This LNP-based delivery system holds promise for further development as a gene therapy strategy for familial hypercholesterolemia.

Ethics approval

Not required.

Acknowledgments

The researchers extend their deepest gratitude to the PAMITRAN-UP (Pusat Akademik, Inovasi, Teknologi, dan Riset Kesehatan-Universitas Padjadjaran, Bandung-Indonesia) for providing Hepa1-6 cells; the ITB-Olympus Bioimaging Center (IOBC), Institut Teknologi Bandung (ITB), for access to their advanced equipment the FV1200 confocal laser scanning microscope from Olympus Life Science; and the Research Center for Nanoscience and Nanotechnology (RCNN), Institut Teknologi Bandung (ITB), for the equipment of Nano Particle Analyzer Horiba SZ-100 and Hitachi HT-7700 for nanoparticle assay.

Competing interests

All the authors declare that there are no conflicts of interest.

Funding

This research was funded by Beasiswa Pendidikan Indonesia (BPI) (Grant number: 202101121093) the Center for Higher Education Funding and Assessment (PPAPT) – the Ministry of Higher Education, Science, and Technology of Republic Indonesia; with the Indonesia Endowment Fund for Education Agency (LPDP) – the Ministry of Finance of Republic Indonesia; and also the Research, Community Service, and Innovations Programme (P_2MI) Institut Teknologi Bandung (ITB) that also has provided financial support for this project (Grant number: 16A/IT1.C10/SK-KP/2022).

Underlying data

All data generated in this study are included in the published article and supplementary files (https://doi.org/10.6084/m9.figshare.28426100).

Declaration of artificial intelligence use

We hereby confirm that no artificial intelligence (AI) tools or methodologies were utilized at any stage of this study, including during data collection, analysis, visualization, or manuscript preparation. All work presented in this study was conducted manually by the authors without the assistance of AI-based tools or systems.

How to cite

Prasetia I GNJA, Kurniati NF, Riani C, Mudhakir D. Design of lipid nanoparticle (LNP) containing genetic material CRISPR/Cas9 for familial hypercholesterolemia. Narra J 2025; 5 (1): e2217 - http://doi.org/10.52225/narra.v5i1.2217.

References

1. Kalra S, Chen Z, Deerochanawong C, *et al.* Familial hypercholesterolemia in asia pacific: A review of epidemiology, diagnosis, and management in the region. J Atheroscler Thromb 2021;28(5):417-434.
2. Jackson CL, Zordok M, Kullo IJ. Familial hypercholesterolemia in Southeast and East Asia. Am J Prev Cardiol 2021;6(2):100157.
3. Di Taranto MD, Giacobbe C, Fortunato G. Familial hypercholesterolemia: A complex genetic disease with variable phenotypes. Eur J Med Genet 2020;63(4):103831.
4. Rade N. Pejic. Familial hypercholesterolemia. Ochsner J 2014;14(4):669-672.
5. Bouhairie VE, Goldberg AC. Familial hypercholesterolemia. Cardiol Clin 2015;33(2):169-179.
6. Lau CH. Applications of CRISPR-Cas in bioengineering, biotechnology, and translational research. CRISPR J 2018;1(6):379-404.
7. Knott GJ, Doudna JA. CRISPR-Cas guides the future of genetic engineering. Science 2018;361(6405):866-869.
8. Li L, Hu S, Chen X. Non-viral delivery systems for CRISPR/Cas9-based genome editing: Challenges and opportunities. Biomaterials 2018;171:207-218.
9. Hanna E, Rémuzat C, Auquier P, *et al.* Gene therapies development: Slow progress and promising prospect. J Mark Access Health Policy 2017;5(1):1265293.
10. Sander JD, Joung JK. CRISPR-Cas systems for editing, regulating and targeting genomes. Nat Biotechnol 2014;32(4):347-350.
11. Omer L, Hudson EA, Zheng S, *et al.* CRISPR correction of a homozygous low-density lipoprotein receptor mutation in familial hypercholesterolemia induced pluripotent stem cells. Hepatol Commun 2017;1(9):886-898.
12. Huang L, Hua Z, Xiao H, *et al.* CRISPR/Cas9-mediated ApoE -/- and LDLR -/- double gene knockout in pigs elevates serum LDL-C and TC levels. Oncotarget 2017;8(23):37751-37760.
13. Cencic R, Miura H, Malina A, *et al.* Protospacer adjacent motif (PAM)-distal sequences engage CRISPR Cas9 DNA target cleavage. PLoS ONE 2014;9(10):e109213.
14. Zhang S, Shen J, Li D, *et al.* Strategies in the delivery of Cas9 ribonucleoprotein for CRISPR/Cas9 genome editing. Theranostics 2020;11(2):614-648.
15. Salvi VR, Pawar P. Nanostructured lipid carriers (NLC) system: A novel drug targeting carrier. J Drug Deliv Sci Technol 2019;51(990):255-267.
16. García-Pinel B, Porras-Alcalá C, Ortega-Rodríguez A, *et al.* Lipid-based nanoparticles: Application and recent advances in cancer treatment. Nanomaterials 2019;9(4):638.
17. Hou X, Zaks T, Langer R, *et al.* Lipid nanoparticles for mRNA delivery. Nat Rev Mater 2021;6(12):1078-1094.
18. Erasmus JH, Khandhar AP, Guderian J, *et al.* A nanostructured lipid carrier for delivery of a replicating viral rna provides single, low-dose protection against Zika. Mol Ther 2018;26(10):2507-2522.
19. Chen F, Alphonse M, Liu Q. Strategies for nonviral nanoparticle-based delivery of CRISPR/Cas9 therapeutics. Wiley Interdiscip Rev Nanomed Nanobiotechnol 2020;12(3):e1609.
20. Allen TM, Hansen C, Martin F, *et al.* Liposomes containing synthetic lipid derivatives of poly(ethylene glycol) show prolonged circulation half-lives in vivo. Biochim Biophys Acta Biomembr 1991;1066(1):29-36.
21. Milla P, Dosio F, Cattel L. PEGylation of proteins and liposomes: A powerful and flexible strategy to improve the drug delivery. Curr Drug Metab 2012;13(1):105-119.
22. Sato T, Sakai H, Sou K, *et al.* Poly(ethylene glycol)-conjugated phospholipids in aqueous micellar solutions: Hydration, static structure, and interparticle interactions. J Phys Chem B 2007;111(6):1393-1401.

23. Zhao H, Li Y, He L, *et al.* In vivo AAV-CRISPR/Cas9–mediated gene editing ameliorates atherosclerosis in familial hypercholesterolemia. Circulation 2020;141(1):67-79.
24. Xu S, Weng J. Familial hypercholesterolemia and atherosclerosis: Animal models and therapeutic advances. Trends Endocrinol Metab 2020;31(5):331-333.
25. Brandts J, Dharmayat KI, Ray KK, *et al.* Familial hypercholesterolemia: Is it time to separate monogenic from polygenic familial hypercholesterolemia? Curr Opin Lipidol 2020;31(3):111-118.
26. Jiang L, Wang LY, Cheng X shu. Novel approaches for the treatment of familial hypercholesterolemia: Current status and future challenges. J Atheroscler Thromb 2018;25(8):665-673.
27. Ran FA, Hsu PD, Wright J, *et al.* Genome engineering using the CRISPR-Cas9 system. Nat Protoc 2013;8(11):2281-2308.
28. Paix A, Folkmann A, Rasoloson D, *et al.* High efficiency, homology-directed genome editing in *Caenorhabditis elegans* using CRISPR/Cas9 ribonucleoprotein complex. Genetics 2015;201(1):47-54.
29. Oh SA, Senger K, Madireddi S, *et al.* High-efficiency nonviral CRISPR/Cas9-mediated gene editing of human T cells using plasmid donor DNA. J Exp Med 2022;219(5):1-18.
30. Brinkman EK, Kousholt AN, Harmsen T, *et al.* Easy quantification of template-directed CRISPR/Cas9 editing. Nucleic Acids Res 2018;46(10):e58-e58.
31. Mehta M, Bui TA, Yang X, *et al.* Lipid-based nanoparticles for drug/gene delivery: An overview of the production techniques and difficulties encountered in their industrial development. ACS Mater Au 2023;3(6):600-619.
32. Dąbrowska M, Nowak I. Lipid nanoparticles loaded with selected iridoid glycosides as effective components of hydrogel formulations. Materials 2021;14(15):1-23.
33. Khanam T, Syuhada Wan Ata WN, Rashedi A. Particle size measurement in waste water influent and effluent using particle size analyzer and quantitative image analysis technique. Adv Mater Res 2016;1133:571-575.
34. Uysal I, Severcan F, Evis Z. Characterization by Fourier transform infrared spectroscopy of hydroxyapatite co-doped with zinc and fluoride. Ceram Int 2013;39(7):7727-7733.
35. Paunovska K, Sago CD, Monaco CM, *et al.* A direct comparison of in vitro and in vivo nucleic acid delivery mediated by hundreds of nanoparticles reveals a weak correlation. Nano Lett 2018;18(3):2148-2157.
36. Cai L, Qin X, Xu Z, *et al.* Comparison of cytotoxicity evaluation of anticancer drugs between real-time cell analysis and CCK-8 method. ACS Omega 2019;4(7):12036-12042.
37. Tang ZZ, Zhang YM, Zheng T, *et al.* Sarsasapogenin alleviates diabetic nephropathy through suppression of chronic inflammation by down-regulating PAR-1: In vivo and in vitro study. Phytomedicine 2020;78(6):153314.
38. Rennick JJ, Johnston APR, Parton RG. Key principles and methods for studying the endocytosis of biological and nanoparticle therapeutics. Nat Nanotechnol 2021;16(3):266-276.
39. Schindelin J, Arganda-Carreras I, Frise E, *et al.* Fiji: An open-source platform for biological-image analysis. Nat Methods 2012;9(7):676-682.
40. Mudhakir D, Akita H, Tan E, *et al.* A novel IRQ ligand-modified nano-carrier targeted to a unique pathway of caveolar endocytic pathway. J Controlled Release 2008;125(2):164-173.
41. Wang T, Larcher LM, Ma L, *et al.* Systematic screening of commonly used commercial transfection reagents towards efficient transfection of single-stranded oligonucleotides. Molecules 2018;23(10):2564.
42. Rahimi P, Mobarakeh VI, Kamalzare S, *et al.* Comparison of transfection efficiency of polymer-based and lipid-based transfection reagents. Bratisl Med J 2018;119(11):701-705.
43. Shi B, Xue M, Wang Y, *et al.* An improved method for increasing the efficiency of gene transfection and transduction. Int J Physiol Pathophysiol Pharmacol 2018;10(2):95-104.
44. Severino P, Andreani T, Macedo AS, *et al.* Current state-of-art and new trends on lipid nanoparticles (SLN and NLC) for oral drug delivery. J Drug Deliv 2012;2012:1-10.
45. Das S, Chaudhury A. Recent advances in lipid nanoparticle formulations with solid matrix for oral drug delivery. AAPS PharmSciTech 2011;12(1):62-76.
46. Karn-Orachai K, Smith SM, Phunpee S, *et al.* The effect of surfactant composition on the chemical and structural properties of nanostructured lipid carriers. J Microencapsul 2014;31(6):609-618.
47. Oktay AN, Ilbasmis-Tamer S, Celebi N. The effect of critical process parameters of the high pressure homogenization technique on the critical quality attributes of flurbiprofen nanosuspensions. Pharm Dev Technol 2019;24(10):1278-1286.
48. Agrahari V, Kabra V, Trivedi P. Development, optimization and characterization of nanoparticle drug delivery system of cisplatin. In: Lim CT, Goh JCS, editors. 13th International Conference on Biomedical Engineering (IFMBE). Heidelberg: Springer Berlin; 2009.

49. Tungadi R. The effect of ultrasonication time on particle size, polydispersity index and stability evaluation of anthocyanin liposomes. Univers J Pharm Res 2024;9(1):8-13.
50. Anderson W, Kozak D, Coleman VA, *et al.* A comparative study of submicron particle sizing platforms: Accuracy, precision and resolution analysis of polydisperse particle size distributions. J Colloid Interface Sci 2013;405:322-330.
51. Clayton KN, Salameh JW, Wereley ST, *et al.* Physical characterization of nanoparticle size and surface modification using particle scattering diffusometry. Biomicrofluidics 2016;10(5):054107.
52. Vllasaliu D, Fowler R, Stolnik S. PEGylated nanomedicines: Recent progress and remaining concerns. Expert Opin Drug Deliv 2014;11(1):139-154.
53. Chun W, Zhanzhan Z, Yang L. Recent progress on nonviral delivery carriers for CRISPR/Cas9 systems. Mater Matters 2020;15(3):104-111.
54. El-Sayed A, Futaki S, Harashima H. Delivery of macromolecules using arginine-rich cell-penetrating peptides: Ways to overcome endosomal entrapment. AAPS J 2009;11(1):13-22.
55. Urban-Klein B, Werth S, Abuharbeid S, *et al.* RNAi-mediated gene-targeting through systemic application of polyethylenimine (PEI)-complexed siRNA in vivo. Gene Ther 2005;12(5):461-466.
56. Luo Y, Chen D, Ren L, *et al.* Solid lipid nanoparticles for enhancing vinpocetine's oral bioavailability. J Controlled Release 2006;114(1):53-59.
57. Danhier F, Ansorena E, Silva JM, *et al.* PLGA-based nanoparticles: An overview of biomedical applications. J Controlled Release 2012;161(2):505-522.
58. Bhattacharjee S. DLS and zeta potential - What they are and what they are not? J Controlled Release 2016;235:337-351.
59. Ciani L, Ristori S, Salvati A, *et al.* DOTAP/DOPE and DC-Chol/DOPE lipoplexes for gene delivery: Zeta potential measurements and electron spin resonance spectra. Biochim Biophys Acta 2004;1664(1):70-79.
60. Kong W, Wei Y, Dong Z, *et al.* Role of size, surface charge, and PEGylated lipids of lipid nanoparticles (LNPs) on intramuscular delivery of mRNA. J Nanobiotechnology 2024;22(1):553.
61. Ewe A, Höbel S, Heine C, *et al.* Optimized polyethylenimine (PEI)-based nanoparticles for siRNA delivery, analyzed in vitro and in an ex vivo tumor tissue slice culture model. Drug Deliv Transl Res 2017;7(2):206-216.
62. Filipe V, Hawe A, Jiskoot W. Critical evaluation of nanoparticle tracking analysis (NTA) by NanoSight for the measurement of nanoparticles and protein aggregates. Pharm Res 2010;27(5):796-810.
63. Schultz D, Münter RD, Masi A, *et al.* Enhancing RNA encapsulation quantification in lipid nano-particles: Sustainable alternatives to Triton X-100 in the Ri-boGreen Assay. Eur J Pharm Biopharm 2024;205(4):114571.
64. Park SA, Ahn JB, Choi SH, *et al.* The effects of particle size on the physicochemical properties of optimized astaxanthin-rich Xanthophyllomyces dendrorhous-loaded microparticles. LWT 2014;55(2):638-644.
65. Astete CE, Sabliov CM. Synthesis and characterization of PLGA nanoparticles. J Biomater Sci Polym Ed 2006;17(3):247-289.
66. Silva AH, Filippin-Monteiro FB, Mattei B, *et al.* In vitro biocompatibility of solid lipid nanoparticles. Sci Total Environ 2012;432:382-388.
67. Nassimi M, Schleh C, Lauenstein HD, *et al.* Low cytotoxicity of solid lipid nanoparticles in in vitro and ex vivo lung models. Inhal Toxicol 2009;21(Suppl 1):104-109.
68. Kim MW, Kwon SH, Choi JH, *et al.* A promising biocompatible platform: Lipid-based and bio-inspired smart drug delivery systems for cancer therapy. Int J Mol Sci 2018;19(12):1-20.
69. Partearroyo MA, Ostolaza H, Goñi FM, *et al.* Surfactant-induced cell toxicity and cell lysis. A study using B16 melanoma cells. Biochem Pharmacol 1990;40(6):1323-1328.
70. Durán-Lobato M, Martín-Banderas L, Lopes R, *et al.* Lipid nanoparticles as an emerging platform for cannabinoid delivery: Physicochemical optimization and biocompatibility. Drug Dev Ind Pharm 2016;42(2):190-198.
71. Petersen S, Steiniger F, Fischer D, *et al.* The physical state of lipid nanoparticles influences their effect on in vitro cell viability. Eur J Pharm Biopharm 2011;79(1):150-161.
72. Winter E, Pizzol CD, Locatelli C, *et al.* Development and evaluation of lipid nanoparticles for drug delivery: Study of toxicity in vitro and in vivo. J Nanosci Nanotechnol 2016;16(2):1321-1330.
73. Donahue ND, Acar H, Wilhelm S. Concepts of nanoparticle cellular uptake, intracellular trafficking, and kinetics in nanomedicine. Adv Drug Deliv Rev 2019;143:68-96.
74. Liu P, Sun Y, Wang Q, *et al.* Intracellular trafficking and cellular uptake mechanism of mPEG-PLGA-PLL and mPEG-PLGA-PLL-Gal nanoparticles for targeted delivery to hepatomas. Biomaterials 2014;35(2):760-770.

75. Hu J, Zhang Z, Shen WJ, *et al.* Cellular cholesterol delivery, intracellular processing and utilization for biosynthesis of steroid hormones. Nutr Metab 2010 71 2010;7(1):1-25.
76. Chatterjee S, Kon E, Sharma P, *et al.* Endosomal escape: A bottleneck for LNP-mediated therapeutics. Proc Natl Acad Sci 2024;121(11):1-9.
77. Rai MN, Rhodes B, Jinga S, *et al.* Efficient mutagenesis of maize inbreds using biolistics, multiplex CRISPR/Cas9 editing, and Indel-Selective PCR. Plant Mehods 2025;43:1-37.
78. Zhao QQ, Chen JL, Lv TF, *et al.* N/P ratio significantly influences the transfection efficiency and cytotoxicity of a polyethylenimine/chitosan/DNA complex. Biol Pharm Bull 2009;32(4):706-710.
79. Prabha S, Arya G, Chandra R, *et al.* Effect of size on biological properties of nanoparticles employed in gene delivery. Artif Cells Nanomed Biotechnol 2016;44(1):83-91.
80. Ishii T, Okahata Y, Sato T. Mechanism of cell transfection with plasmid/chitosan complexes. Biochim Biophys Acta 2001;1514(1):51-64.
81. Abidin M, Yusuf M, Widayat W, *et al.* The implementation of response surface methodology in the optimization of lipid nanoparticle preparation for vaccine development. Trends Sci 2023;21(1):7142.
82. Richardson CD, Ray GJ, DeWitt MA, *et al.* Enhancing homology-directed genome editing by catalytically active and inactive CRISPR-Cas9 using asymmetric donor DNA. Nat Biotechnol 2016;34(3):339-344.
83. Chen H, Neubauer M, Wang JP. Enhancing HR frequency for precise genome editing in plants. Front Plant Sci 2022;13(5):883421.
84. Mou H, Smith JL, Peng L, *et al.* CRISPR/Cas9-mediated genome editing induces exon skipping by alternative splicing or exon deletion. Genome Biol 2017;18(1):4-11.
85. Liu J, Chang J, Jiang Y, *et al.* Fast and efficient CRISPR/Cas9 genome editing in vivo enabled by bioreducible lipid and messenger RNA nanoparticles. Adv Mater 2019;31(33):1-7.
86. Franceschi RT, Yang S, Rutherford RB, *et al.* Gene therapy approaches for bone regeneration. Cells Tissues Organs 2004;176(1-3):95-108.
87. Kim TK, Eberwine JH. Mammalian cell transfection: The present and the future. Anal Bioanal Chem 2010;397(8):3173-3178.
88. Hussain W, Mahmood T, Hussain J, *et al.* CRISPR/Cas system: A game changing genome editing technology, to treat human genetic diseases. Gene 2019;685:70-75.
89. Islam MT, Molla KA. CRISPR-Cas methods. New York: Springer; 2020.
90. Suzuki KIT, Hayashi T. Targeted genome editing using site-specific nucleases. Tokyo: Springer Japan; 2015.
91. Chen R, Huang H, Liu H, *et al.* Friend or foe? Evidence indicates endogenous exosomes can deliver functional gRNA and Cas9 protein. Small J 2019;15(38):1-13.